**Discover** Atmosphere

Research

# Characterizing and sourcing metal air contamination coupling concentrations and lead isotopes from moss biomonitoring in urban cemeteries

**David Widory[1] · Caroline Meyer[2] · Sébastien Leblond[2] · Edson Plasencia Sánchez[3] · Emeline Lequy[4] · Yasser Morera-Gómez[1,5]**

Received: 6 September 2024 / Accepted: 21 November 2024
Published online: 02 December 2024
© The Author(s) 2024 OPEN

**Abstract**
Populations are constantly exposed to airborne metals, in particular in urban areas. Despite their proven links to health issues, their origin and fate are still subject to debate. Bioindicators, by taking up and cumulating atmospheric metals over time, have been widely used to proxy environmental quality over large areas, at various time scales. Using the example of the Paris region, we investigated the potential for the *Grimmia pulvinata* moss species to both characterize air metal contamination and to identify its main sources. To this end, we coupled metal/metalloid (Al, As, Cd, Cr, Cu, Fe, Ni, Pb, Sb, Sr, V and Zn) concentrations and Pb isotope ratios from samples collected in cemeteries in the city and its suburbs. Metal enrichment factors ranged between 2 and 10 for As, Cr, Fe, Ni, Sr, V, between 50 and 100 for Cu, Pb and Zn and > 100 for Cd and Sb, indicating a dominant anthropogenic origin. Principal component analysis showed that 3 principal components explained 89% of the metal variations: (i) European atmospheric background, (ii) regional urban sources, and (iii) resuspension of regional soils. This was corroborated by Pb isotope ratios, whose variations were modelled by a ternary mixing that considered the same 3 emission sources. Using a MixSIAR isotope model, we reveal that the European atmospheric background contributes slightly (< ~ 5%) and that within 20 km of the city center bioindicators are mostly impacted by urban sources (contributions: 50–80%). Samples collected > 20 km show almost equal contributions of the endmembers representing urban activities and agricultural soil resuspension.

**Keywords** Bioindicators · Air pollution · *Grimmia pulvinata* · Metals · Pb isotopes

**Supplementary Information** The online version contains supplementary material available at https://doi.org/10.1007/s44292-024-00022-6.

✉ David Widory, widory.david@uqam.ca | [1]Geotop/Université du Québec à Montréal (UQAM), 201 Ave Président Kennedy, Montréal, QC H2X 3Y7, Canada. [2]PatriNat (OFB-MNHN-CNRS-IRD), 12 Rue Buffon, 75005 Paris, France. [3]Grup MAiMA, SGR Mineralogia Aplicada, Geoquímica i Geomicrobiologia, Department de Mineralogia, Petrologia i Geologia Aplicada, Facultat de Ciències de la Terra, Institut de Recerca de l'Aigua (IdRA), Universitat de Barcelona (UB), Martí Franquès S/N, 08028 Barcelona, Spain. [4]Unité "Cohortes en Population" UMS 011 Inserm/Université Paris-Cité/Université Paris Saclay/UVSQ, Villejuif, France. [5]Universidad de Navarra, Instituto de Biodiversidad y Medioambiente BIOMA, Irunlarrea 1, 31008 Pamplona, Spain.

## 1 Introduction

Air pollution, a worldwide major contributing factor to the global burden of disease (e.g., [1, 2]), remains especially high in urban areas. Heavy metals in the urban atmosphere originate from various human sources, from traffic to current or past industrial legacy. Even less industrialized atmospheres can be negatively affected by ubiquitous historical pollution sources (e.g., [3]). Lead (Pb) is a (neuro)toxic metal that adversely impacts human health, especially at great intake rates [4]. Chronic low-level exposure to Pb has been investigated for many health outcomes, including cognitive development or decline [5, 6]. Although atmospheric Pb contamination has dramatically decreased since the regulatory phasing out of one of its major emission sources, i.e., tetraethyl lead additives in leaded gasoline, and of other leaded products worldwide (e.g., [7, 8]), Pb can be retained in soils and dusts for decades, with possible resuspension in the air, and thus potentially continues to harm human health (e.g., [9–11]).

Since the pioneer biomonitoring network established in Sweden in 1975 [12], lichens and mosses have been widely used as bio-proxies to monitor the distribution and concentration of airborne pollutants [13]. Due to the lack of root and of developed conducting tissue system, most terrestrial mosses absorb water and nutrients, but also simultaneously pollutants, directly from the atmosphere. Pollutants can be preserved in moss for long periods of time [14]. Despite some remaining uncertainties such as the duration of metal retention and the chemical forms of metals, mosses are considered better biomonitors for heavy metal pollution than vascular plant leaves for long time periods, as they can accumulate more metals (3 to 51 times more; [15]) and are also well suited for passive biomonitoring in urban settings.

Pb has 4 stable isotopes ($^{204}$Pb, $^{206}$Pb, $^{207}$Pb and $^{208}$Pb) that have been widely studied for several purposes, such as monitoring Pb accumulation in the environment (e.g., [16]) as well as tracing its origin(s) (e.g., [17, 18]), including in bioindicators (e.g., [19–21]). This approach is based on the possibility for Pb isotope ratios to discriminate most of atmospheric emission sources by their specific isotope signatures (e.g., [22]). For example, [23] recently defined the Pb characteristic isotope signatures for the major urban emission sources as follows: road traffic ($^{206}$Pb/$^{207}$Pb = 1.146 ± 0.005; $^{208}$Pb/$^{207}$Pb = 2.418 ± 0.009), petrol industry ($^{206}$Pb/$^{207}$Pb = 1.148 ± 0.009; $^{208}$Pb/$^{207}$Pb = 2.292 ± 0.008), coal-fired facilities ($^{206}$Pb/$^{207}$Pb = 1.159 ± 0.004; $^{208}$Pb/$^{207}$Pb = 2.467 ± 0.006) and oil-fired facilities ($^{206}$Pb/$^{207}$Pb = 1.126 ± 0.004; $^{208}$Pb/$^{207}$Pb = 2.278 ± 0.005). Pb isotopes are not fractionated by plants [24], making them an interesting tool to identify sources of airborne pollution in mosses. Several studies have shown that Pb isotopes in pleurocarpous mosses allow identifying the corresponding Pb emission sources and highlighting regional variations among them [25–27]. Although most studies have focused on rural environments and on large scales (national and international), studies more specific to the urban environment have shown that Pb isotopes in mosses are efficient at discriminating between sources as well as between urban sectors [28, 29]. While the studies carried out in urban environments are using either moss-bag [26] or pleurocarpous mosses [28, 30], it is noteworthy that mosses with a cushion morphology are more abundant in urban environments. For this study we selected *Grimmia pulvinata*, a species commonly used for the determination of metals [31–33]. To our knowledge, *Grimmia pulvinata* has only been characterized for its radioactive $^{210}$Pb activity [34] but never for its primordial ($^{204}$Pb) and radiogenic ($^{206}$Pb, $^{207}$Pb and $^{208}$Pb) isotopes.

Here, we investigated the concentrations of 12 metals and metalloids, and the corresponding Pb stable isotope ratios in *Grimmia pulvinata* moss samples that had been previously collected in cemeteries in Paris (France) and its vicinity [31, 32]. The objectives of this study were multiple: (i) to characterize the level of metal contamination in the atmosphere of the Parisian region, (ii) to identify the corresponding emission source(s) and its/their relative contribution(s) in this area, and iii) to evaluate the potential of this approach to be implemented in other cities worldwide.

## 2 Methods

### 2.1 *Grimmia pulvinata* as urban passive moss biomonitors

*Grimmia pulvinata* (Hedw.) Sm. (Grimmiaceae, Grimmiales) is a common acrocarpous moss that forms hoary, greyish-green cushions. The epithet "pulvinata" refers to the cushion-like appearance of the plants. *Grimmia pulvinata* seems

suited for biomonitoring airborne metals [35] in urban areas, including in cemeteries [33]. *Grimmia pulvinata* is distributed worldwide. It is ubiquitous in temperate regions at altitudes up to ~ 3000 m. We elected to collect bioindicators in cemeteries as: (i) they are widely spread in the Paris region (14 within the capital city and 6 in its vicinity), (ii) they shelter mosses [33], (iii) they enable the collection of moss samples directly exposed to atmospheric deposition in absence of obstacles such as vegetation, and (iv) they offer homogeneous substrates such as concrete.

### 2.2 Sampling

The sampling strategy and collection protocol are detailed elsewhere [31, 32]. In brief, moss samples were collected in May 2018 in 77 cemeteries located in Paris and in an area within a radius of ~ 70 km from the city center (Fig. 1A). Only mosses with a cushion diameter between 3 and 5 cm were taken, ensuring that all samples have approximately the same age. Collection was made following standardized methods on concrete substrates, either on tombstones or on the top of walls, avoiding decorative metallic objects. An average of 75 moss colonies (minimum 50) on at least 10 tombstones, or on a total length of 15 m on top of two distinct walls, were sampled to minimize the potential influence of local contamination. Concrete was chosen as it presents a low risk of contamination. A total of about 9600 cushions were collected. Each cushion was validated with a magnifying glass (10× magnification). In the laboratory, samples were dried at room temperature, manually cleaned, subjected to routine grinding with an automatic non-polluting titanium grinder (Pulverisette 14, Fritsch, Germany) and stored for further analysis. Sampling and preparation were conducted using nytril gloves and ceramic knives to avoid any metal contamination.

The same subset of 77 samples recently studied by [31] was selected for the purpose of this study. In brief, [31] developed a target-style gridded map based on concentric circles originating from the city center and covering the Ile-de-France region. These circles are crossed by transects starting from the city center and passing through areas with the highest possible population density, while covering as many directions as possible. The junctions between circles and transects defined the potential sampling sites.

### 2.3 Metal concentrations and Pb isotope analysis

Twelve metals/metalloids (Al, Cu, Fe, Sr, Zn, As, Cd, Cr, Ni, Pb, Sb, V) were quantified after drying at 40 °C and acid (HF, $HNO_3$, $H_2O_2$) digestion. Measurements were made at the USRAVE laboratory (INRAE, Bordeaux). This laboratory is accredited by the French accreditation committee COFRAC for measuring metals in plants (NF EN ISO/IEC 17025). Al, Cu, Fe, Sr and Zn concentrations were measured by inductively coupled plasma atomic emission spectrometry ICP-AES (ICP-AES Varian 725ES spectrometer), whereas other elements (As, Cd, Cr, Ni, Pb, Sb and V) were quantified by inductively coupled plasma mass spectrometry ICPMS (Agilent 7700 × spectrometer). Concentrations are expressed at 103 °C and were corrected for water loss (determined on a subsample). The USRAVE laboratory provides concentrations with analytical uncertainties of 20% for As, Cd, Cu, Cr, Ni, Sb and Pb, 15% for Al and Fe and 10% for Zn. Certified reference materials (CRMs) NIST 1547 (peach leaves), NIST 1573a (tomato leaves), as well as European moss survey reference materials Moss M2 and Moss M3 were processed with each sample batch. Moss M2 and Moss M3 standards are *Pleurozium schreberi* (Willd. ex Brid.) Mitt. powders from two Finnish sites [37].

For Pb isotope analysis, all moss samples were prepared at the Geotop clean laboratory (class-100) in Montreal. Pb digestion and chemical purification followed the procedure described in [19]. In brief, 50 mg of moss sample were placed in pre-cleaned Teflon bombs. Samples were digested with concentrated HCl, $HNO_3$ (1:2) for 3–4 days at 100 °C. Upon complete digestion, the solution was evaporated to dryness at 60–70 °C and 1 mL of HBr was added. The solution was ultrasonicated for 1 h. Finally, Pb was extracted by resin chromatography before isotope analysis. The Pb isotope ratios ($^{206}Pb/^{204}Pb$, $^{207}Pb/^{204}Pb$, $^{208}Pb/^{204}Pb$, $^{207}Pb/^{206}Pb$ and $^{208}Pb/^{206}Pb$) were measured by MC-ICP-MS on a NuPlasma II with an Aridus II desolving membrane as the introduction system. All samples were doped with thallium (Tl) to correct for the mass bias (e.g., [38]). Calibration and isotope correction factor were operated using a standard-sample bracketing technique: the NIST SRM 981 pure Pb standard was measured every 5 samples throughout the analytical sequence. Concentrations of the NIST SRM 981 solutions were adjusted to match the Pb signal intensity of our samples, in order to minimize any mass bias potentially induced by the matrix effect. External organic matrices lichen standard references IAEA-336, BCR482; minerals standard references BCR-1, BHVO2; and a pure Pb solution CGPB-1 (repeatedly measured on our MC-ICP-MS for several years) were also measured within each analytical batch. USGS BCR-1 and BHVO2 mineral basaltic glass standards were digested with high purity hydrofluoric (HF) and nitric ($HNO_3$) acids at 100 °C on a hot plate. For BCR-1 average isotope ratios were (n = 12) $^{208}Pb/^{204}Pb = 38.769 \pm 0.092$, $^{207}Pb/^{204}Pb = 15.648 \pm 0.035$,

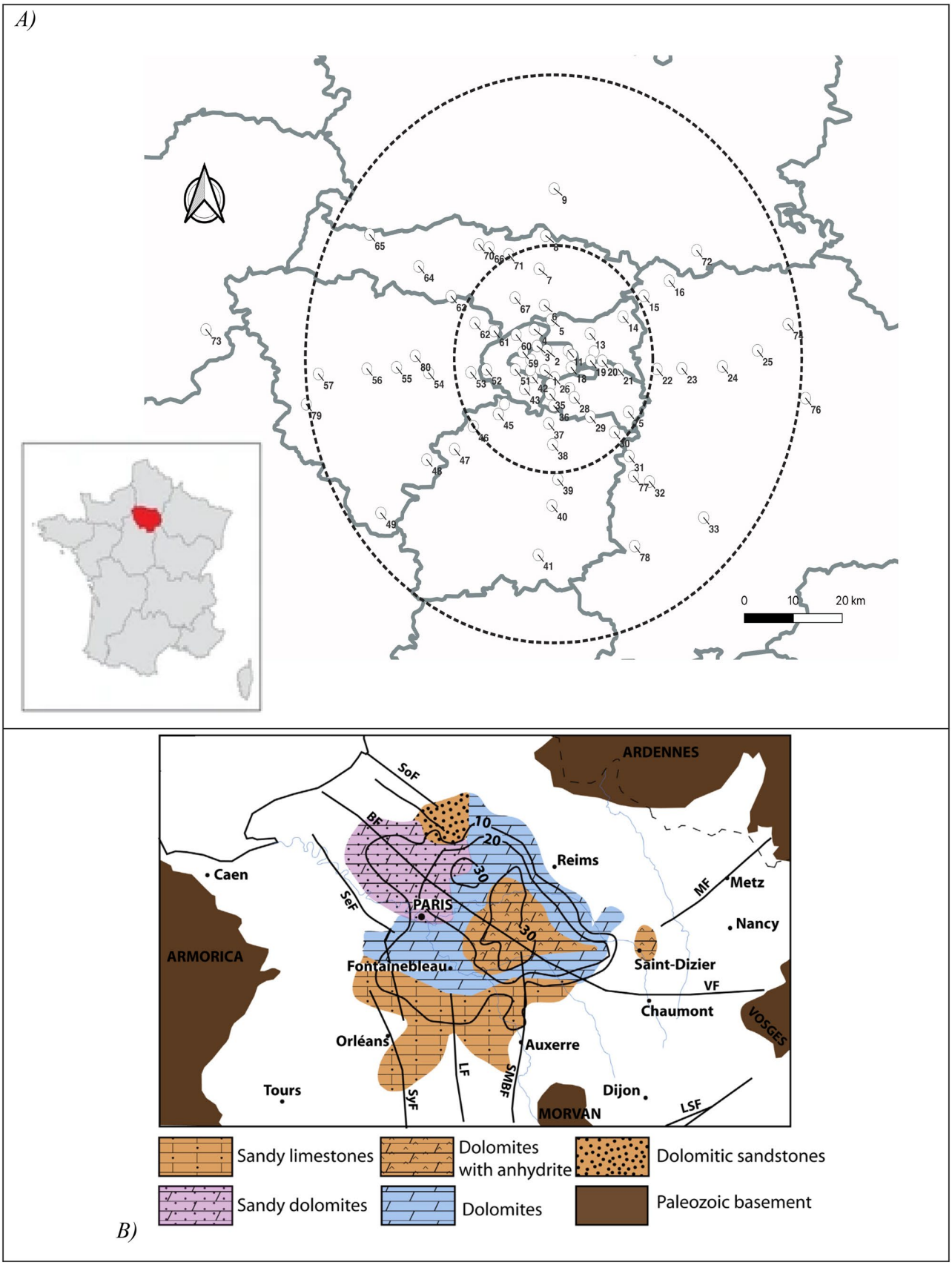



**Fig. 1** **A** Map showing Grimmia pulvinata moss sampling locations in Paris and its vicinity. Dashed circles represent the 20 and 50 km-radius circles from the center of Paris. Numbers correspond to sampling sites listed in Table S1. **B** Simplified geological map of the sedimentary Paris Basin (adapted from [36])

$^{206}Pb/^{204}Pb = 18.807 \pm 0.047$, $^{208}Pb/^{206}Pb = 2.061 \pm 0.002$, in agreement with the certified values reported by [39]. For BHVO2 (n = 12), $^{208}Pb/^{204}Pb = 38.311 \pm 0.071$, $^{207}Pb/^{204}Pb = 15.559 \pm 0.020$, $^{206}Pb/^{204}Pb = 18.702 \pm 0.030$, $^{208}Pb/^{206}Pb = 2.049 \pm 0.002$, in agreement with [39, 40]. For IAEA336 (n = 12), $^{208}Pb/^{204}Pb = 37.774 \pm 0.086$, $^{207}Pb/^{204}Pb = 15.607 \pm 0.028$, $^{206}Pb/^{204}Pb = 17.837 \pm 0.026$, $^{208}Pb/^{206}Pb = 2.121 \pm 0.002$, similar to [19]. For BCR482 (n = 12), $^{208}Pb/^{204}Pb = 37.519 \pm 0.086$, $^{207}Pb/^{204}Pb = 15.595 \pm 0.029$, $^{206}Pb/^{204}Pb = 17.631 \pm 0.035$, $^{208}Pb/^{206}Pb = 2.131 \pm 0.003$, consistent with previous studies (e.g., [19, 41]).

Procedural blanks (pg Pb blank/ pg Pb sample) were < 5% for all samples and were thus considered negligible.

## 2.4 Data processing

### 2.4.1 Enrichment factors

Enrichment (EF) factors were used to quantify the level of atmospheric pollution in the study area. EF is an indicator that evaluates the contribution of anthropogenic sources to a given element content in bioindicators. EF is calculated as the ratio between the concentration of the considered element ($C_i$) normalized to the concentration of a conservative element ($C_x$) versus the ratio of the same elements in the parent material [42]:

$$EF_i = \frac{\left(\frac{C_i}{C_x}\right)_{sample}}{\left(\frac{C_i}{C_x}\right)_{background}}$$

Aluminum (Al), selected here, is generally used as the conservative element (e.g., [33, 43, 44]). For all calculations, we computed the background elemental concentrations defined by [45] for the upper continental crust (UCC). According to the degree of enrichment, elements may be grouped as follows: no enrichment (EF < 1); minor enrichment (1 < EF < 3); moderate enrichment (3 < EF < 5); moderately severe enrichment (5 < EF < 10); severe enrichment (10 < EF < 25), very severe enrichment (25 < EF < 50); and extremely severe enrichment (EF > 50) [46]. Previous studies have shown that EF values < 10 suggest a greater possibility of a natural crustal origin, whereas values between 10 and 100 should be considered to indicate that human activities and mixed sources (from both natural and anthropogenic sources) are the most probable sources. EF values > 100 are considered to result of anthropogenic sources or exceptional geological events [47, 48].

### 2.4.2 Principal component analysis

The exploratory data analysis aimed at studying the relations existing among the investigated variables was performed using a Principal Component Analysis (PCA) with VARIMAX rotation under R version 4.3.1 (PSYCH package). Prior to the statistical analysis, the data set distribution was evaluated using the Kolmogorov–Smirnov method. When the distribution was not normal (Cd, Cr, Cu, Ni, Pb, Sb, and Zn), the data was log-transformed. For Sr, values were transformed using the Box-Cox transformation ($\lambda = -0.9$). The PCA analysis was applied to our initial dataset after a standardization process. The PCA results were considered valid when the cumulative variance explained by the principal components exceeded 85% of the total variance in the dataset. Based on these criteria, a total of 4 principal components were successfully identified.

### 2.4.3 Isotope mass balance (IMB) and MixSIAR models

We can model mixing relationships for different endmembers using Isotope Mass Balance (IMB) equations and estimate their corresponding contributions for each sample. The mixing equation for a k component system for isotope ratios can be expressed in the following way [49]:

$$I = \frac{\sum_{i=1}^{k} z_i n_i I_i}{\sum_{i=1}^{k} z_i n_i}$$

With $\sum_{i=1}^{k} z_i = 1$ and $0 \le z_i \le 1$, and where I is the isotope ratio in the mixture, $I_i$ the isotope ratio in each endmember component, $z_i$ the mass fraction of component 1, 2, 3… and $n_i$ the relative enrichment of element i in component 1, 2, 3… relative to component k (i.e., $n_i = c_i/c_k$; where c is the concentration of element i).

The MixSIAR Bayesian isotope mixing model [50] has been widely used to quantify the contribution of multiple sources to environmental mixture (e.g., [51]). Compared to previous models, MixSIAR allows for a variable form of source signature and a priori evaluation of the data. This results in better error structure and prediction accuracy [50]. For example, [16] recently used it to source apportion Pb sources based on their isotope signatures in lichen and road sediment in two US urban-industrial centers. Here, $^{204}Pb/^{207}Pb$, $^{206}Pb/^{207}Pb$ and $^{208}Pb/^{207}Pb$ isotope ratios measured in the bioindicator samples were used as input parameters, together with the identified endmembers' Pb isotope signatures.

#### 2.4.4 Correlation analysis

The Spearman correlation tests are a nonparametric test that measures the statistical dependence between the ranking of two variables. They were performed using JMP® Pro 16.

## 3 Results and discussion

### 3.1 Metal concentrations

As previously observed in other studies [31, 32], the highest concentrations were found for the geologically abundant Al (average of 6375 ± 1790 mg/kg) and Fe (average of 5569 ± 2038 mg/kg), followed by Zn, Pb, Cu, Sr, V, Cr, Ni, As, Sb and Cd (Table 1). Compared to the previous study in Paris [33], our concentrations were notably lower for Cr, Ni and Fe, but higher for Al and Pb. Lead concentrations were on average 82 ± 53 mg/kg (Table 1), substantially higher than those of [33]. These discrepancies may be attributed to the differences in the respective moss analytical protocols used. While in [33] moss samples were washed and then digested with $HNO_3$, we did not wash our samples and digested them with multiple acids (HF, $HNO_3$, $H_2O_2$), allowing to analyze both the dust deposited on moss leaves and the metals present in ionic form. For all metals, our concentrations are consistent with those measured in Bilbao, Spain [35], except for Al for which Paris presents higher concentrations. As discussed by [31], the spatial distribution of most metals follows an urban–rural gradient and often seems to be driven by urban-related land use variables, such as the population density or the share of urban area surrounding each sampling site.

**Table 1** Descriptive statistics summary for metal concentrations in the *Grimmia pulvinata* samples

| Metal. | This study (n = 77) | | | | Spain, 2021* | | Paris, France, 2016** |
|---|---|---|---|---|---|---|---|
| | Min | Max | Median | Mean absolute deviation | Min | Max | Mean ± SD |
| Al | 2830 | 12,600 | 6590 | 1436 | 1081 ± 70 | 3610 ± 290 | 2497 ± 123 |
| As | 0.7 | 3.6 | 1.8 | 1 | 1.12 ± 0.18 | 5.0461 ± 0.0074 | 3 ± 1.6 |
| Cd | 0.2 | 2.8 | 0.9 | 1 | 0.59 ± 0.12 | 4.01 ± 0.23 | nd |
| Cr | 4 | 48 | 13 | 6 | 5.6 ± 0.075 | 40.6 ± 3.1 | 644 ± 211 |
| Cu | 9 | 344 | 60 | 38 | 21.3 ± 1.2 | 225 ± 17 | 91 ± 29 |
| Fe | 1640 | 10,600 | 5550 | 1692 | 1992 ± 270 | 12,300 ± 400 | 7314 ± 1153 |
| Ni | 2 | 19 | 7 | 4 | 5 ± 0.33 | 18.9 ± 0.17 | 18 ± 5 |
| Pb | 7 | 265 | 68 | 42 | 16.2 ± 2.5 | 1077 ± 1 | 28 ± 0.6 |
| Sb | 0.4 | 11.1 | 2.7 | 2 | 0.2646 ± 0.0025 | 1.650 ± 0.140 | nd |
| Sr | 36 | 204 | 58 | 19 | 37.5 ± 0.23 | 76.5 ± 0.14 | 44 ± 11 |
| V | 6 | 25 | 16 | 4 | 6.105 ± 0.778 | 18.443 ± 0.103 | 14 ± 8 |
| Zn | 33 | 579 | 209 | 96 | 187 ± 12 | 1750 ± 15 | 205 ± 6 |

Data are compared to other urban passive biomonitoring studies in the literature. Metal concentrations are reported in mg/kg

*nd*: not determined

*[33]: $HNO_3/H_2O_2/H_2O$ digestion; n = 12

**[31]: value for slurry-TXRF leaching; n = 21 (17 samples collected in Paris and 4 in suburban cemeteries)

Spearman correlation tests yielded positive and statistically significant coefficients for all metals except Sr (Figure S1). The highest correlation factor was obtained between Cu and Sb (r = 0.89), elements typically associated with road traffic and wearing from automative brake systems [52, 53], which also strongly suggests an urban origin for these two metals. Other highly positive correlation factors (r ≥ 0.84) were obtained for the Fe–Cr and Fe–Ni pairs, metals usually associated with contaminated soil/dust resuspension in both urban and industrial environments. Additionally, the correlation between Al and Fe (r = 0.81) reinforce the hypothesis of a significant terrigenous contribution of soil-derived material, potentially originating from direct soil contamination or indirect wind-resuspension [54]. Correlation factors of these two soil/dust related elements with As and V (≥ 0.84 and ~ 0.86 with Al and Fe, respectively; Figure S1) were considerably higher than the ones when they are associated to typical fossil fuel or coal combustion elements (≤ 0.39 and ≤ 0.60 with Pb and Zn, respectively; Figure S1). Therefore, a soil (terrigenous) or road traffic (urban) origin is more likely than an industrial one. Pb–Zn, and Pb–Cd yielded more modest correlations (r = 0.66) which may suggest provenance from distinct sources. In contrast, Sr was not significantly correlated to any other metal, suggesting that its budget is independently controlled, most likely by the regional geological carbonate substrates.

### 3.2 Enrichment factors (EF)

Figure 2 shows that metal enrichment factors in *Grimmia pulvinata* vastly vary, from around 2 to EF > 100, suggesting different origins. Fe and Sr yielded average EF of 2 ± 1 and 2 ± 1, respectively, corresponding to a minor enrichment and probably a terrigenous origin, except for one sampling site in Paris for Fe and 15 sites scattered over the study region for Sr. The hypothesis of a Sr contribution from regional carbonate geological substrates is here comforted by the fact that, adding to its aforementioned absence of correlation with the other metals/metalloids, it forms its own principal component in the PCA analysis (see below). It is also consistent with the geology of the local sedimentary Paris basin shown in Fig. 1B. V (average EF = 3 ± 1) is moderately enriched, whereas Ni and Cr are categorised as moderately to moderately severely enriched (average EF of 5 ± 2 and 5 ± 3, respectively). Arsenic, an element known to be toxic [55], is moderately severely to severely enriched. Cu and Zn (both of which are considered biologically essential for living beings under a certain limit, but toxic beyond that limit; [56]) show very severe and extremely severe enrichments (average EF = 57 ± 48 and 52 ± 27, respectively). Some highly toxic metals, including Cd (average EF = 112 ± 57), Sb (average EF = 116 ± 83) and Pb (average EF = 57 ± 37), considered toxic to plants [57], show at least an extremely severe enrichment, thereby highlighting strong respective anthropogenic contributions. The highest lead EF ($EF_{Pb}$) were obtained in the central and western parts of Paris and in its southern suburb (Figure S2). More distant samples mostly yielded lower EF. Our $EF_{Pb}$ range of 6–203 (Table S1), and median value of 47, can be compared to the $EF_{Pb}$ value of ~ 80 calculated for aerosols collected at the Puy de Dôme (central France), one of the defined European regional background sites [58].

### 3.3 Principal component analysis (PCA)

PCA results (Table 2) indicate that the first principal component (PC1) accounts for 37% of the total variability. PC1 is highly positively influenced by the following metals (i.e., loadings > 0.5, from highest to lowest): Sb, Cu, Cr, Cd, Ni, Zn, Fe. PC2 (31%) is influenced by Al, As, V, Fe, Ni, Cr (positive loadings > 0.5). PC3 (15%) is influenced by the positive loadings of Pb (0.90) and Zn (0.64), and moderately by Cd (positive loading of 0.49). Finally, PC4 (9%) is solely influenced by Sr (positive loading of 0.99). PC1 provides a clear gradient from within Paris to its outskirts (Figure S3), with the highest score for sampling site 2 (Montmartre district, most central Parisian site), followed by sampling site 58 (Trocadero square, in front of the Eiffel tower). PC2, PC3 and PC4 are more spatially dispersed. PC2 highest scores are observed in the close and far outskirts (sampling sites 25 and 13, respectively, close to highways, industries, and to a dense rail network). The highest PC3 score corresponds to sampling site 59 (which also yielded the highest $EF_{Pb}$), located in the western outskirt, close to a major traffic road, followed by sampling site 41 in the far southern outskirt (for which the high score remains unexplained), and sampling site 1 in Montparnasse. PC4 highest scores are for sampling sites 52 (southwestern outskirt), 66 and 33 (far north and south outskirts, respectively).

### 3.4 Pb isotope ratios

$^{206}Pb/^{204}Pb$ ratios ranged from 17.87 to 18.29 (average of 18.05 ± 0.09), consistent with the average $^{206}Pb/^{204}Pb$ of 18.132 ± 0.207, reported for *Pseudocleropodium purum* in French forests [59], as well as the isotope ranges reported for urban and French forested areas [60–62]. The $^{206}Pb/^{204}Pb$ range is in the upper range of that measured for *Cladonia*

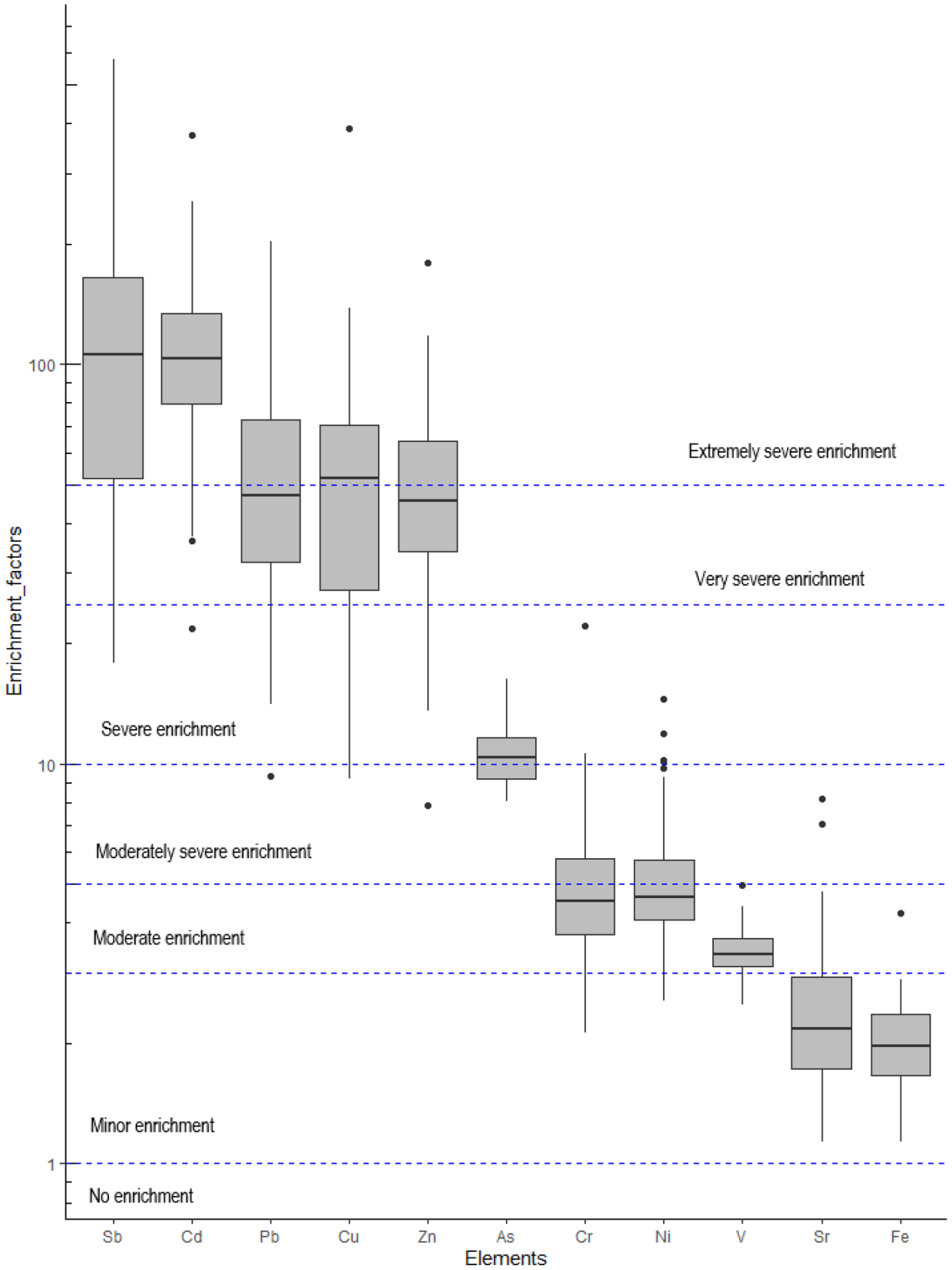



**Fig. 2** Enrichment factors boxplots for the 77 Grimmia pulvinata samples. Aluminium (Al) is used as the reference element in the calculation

*rangiferina* lichens collected along a transect between two smelting complexes in Eastern Canada ($^{206}Pb/^{204}Pb$ from 14.4 to 18.4; [19]), for which the authors determined a background $^{206}Pb/^{204}Pb$ value of 18.2 ± 0.3. In our study, the $^{206}Pb/^{207}Pb$ ratios (ranging from 1.15 to 1.17) are encompassed within the isotope range defined for road traffic (i.e., gasoline exhaust, road dust and tires) in Sao Paulo (Brazil) and Barcelona (Spain), but lower than the typical isotope range the authors

**Table 2** Results of principal component analysis (PCA) with VARIMAX rotation for the *Grimmia pulvinata* samples

| | Communality | PC1 | PC2 | PC3 | PC4 |
|---|---|---|---|---|---|
| Al | 0.93 | 0.17 | 0.93 | 0.10 | 0.18 |
| As | 0.90 | 0.35 | 0.86 | 0.21 | 0.03 |
| Cd | 0.89 | 0.77 | 0.22 | 0.49 | − 0.03 |
| Cr | 0.93 | 0.78 | 0.52 | 0.24 | 0.05 |
| Cu | 0.91 | 0.85 | 0.34 | 0.27 | 0.04 |
| Fe | 0.95 | 0.62 | 0.73 | 0.18 | 0.04 |
| Ni | 0.92 | 0.74 | 0.53 | 0.30 | 0.10 |
| Pb | 0.90 | 0.35 | 0.14 | 0.89 | − 0.06 |
| Sb | 0.94 | 0.89 | 0.31 | 0.23 | 0.02 |
| Sr | 1.00 | 0.04 | 0.15 | − 0.04 | 0.99 |
| V | 0.91 | 0.41 | 0.85 | 0.10 | 0.07 |
| Zn | 0.87 | 0.63 | 0.27 | 0.63 | 0.05 |
| Variance (%) | | 37% | 31% | 15% | 9% |
| Cumulated (%) | | 37% | 68% | 84% | 92% |

defined for industrial emissions in these cities ($^{206}Pb/^{207}Pb > 1.20$) [63]. Our $^{206}Pb/^{207}Pb$ ratios are also higher than the typical range for French gasoline (i.e., 1.07 to 1.13 since the phasing out of leaded gasoline in France in 1990; [64]), and lower than both loess sediments collected in Saclay ($^{206}Pb/^{207}Pb = 1.21$; in the vicinity of sampling site 45) and the background value for the Seine River basin ($^{206}Pb/^{207}Pb = 1.20$) [65]. Our $^{206}Pb/^{207}Pb$ range is however very consistent with that of atmospheric emissions from municipal solid waste incinerators (i.e., $^{206}Pb/^{207}Pb = 1.14–1.15$) hypothesised to represent the typical urban Pb isotope signature in France [65]. Our $^{206}Pb/^{207}Pb$ isotope range is also similar to the $1.167 \pm 0.005$ signature of the fire dust defined by [66], following the fire at Notre Dame Cathedral that happened in Paris in April 2019.

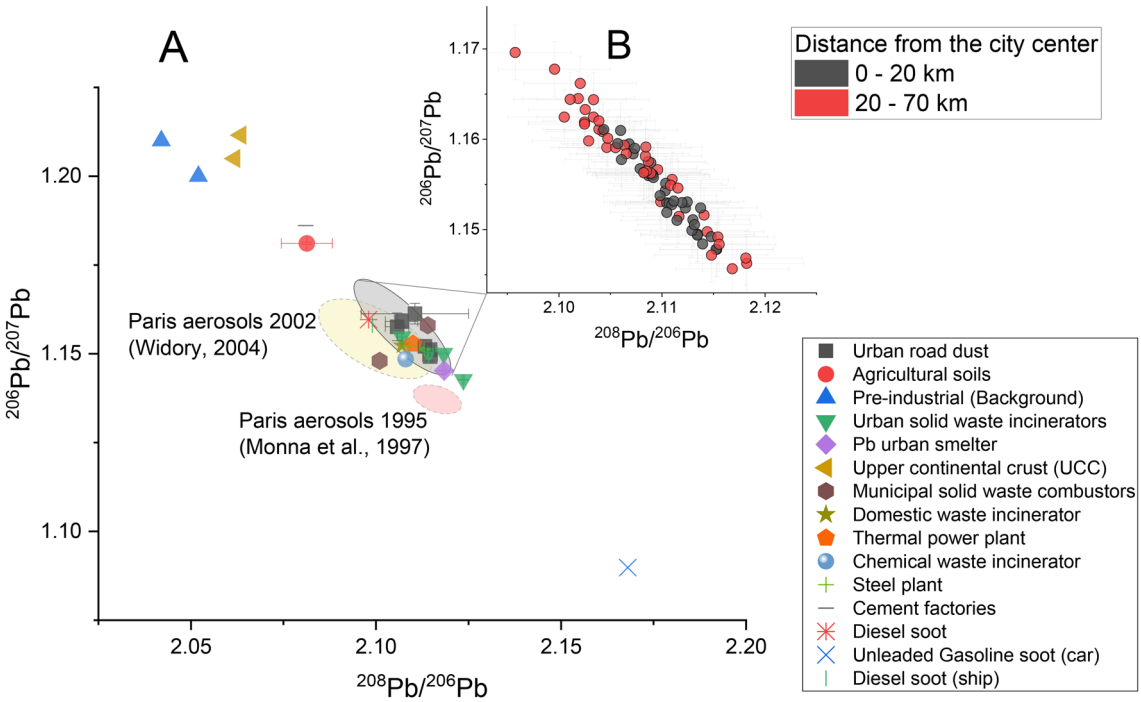



**Fig. 3** Isotope tracking ($^{206}Pb/^{207}Pb$ vs $^{208}Pb/^{206}Pb$) of atmospheric Pb in the Paris region. **A** Potential sources of atmospheric Pb: urban road dust; Agricultural soils and pre-industrial Pb ([65] and references therein); Upper Continental Crust (UCC; [67]); Urban solid waste incinerators and Pb urban smelters [61]; Municipal solid waste combustors [68]; Domestic waste incinerator, thermal power plant, chemical waste incinerator, steel plant, cement factory, diesel soot, unleaded gasoline soot (car) and diesel soot (ship) [69]. The isotope range measured in our moss samples is delineated by the grey oval. **B** Zoom on moss samples (this study)

Pb multi-isotope ratios have been widely applied to moss biomonitoring (e.g., [30]). Here, the classical $^{206}Pb/^{207}Pb$ vs $^{208}Pb/^{206}Pb$ diagram shows that mosses in this study closely align with the contamination mixing line previously defined for France (Fig. 3A). This corroborates our previous hypothesis, based on the observed high $EF_{Pb}$ (Table S1), of a strong impact of emissions from regional industrial activities and road traffic. This is also consistent with the predictive land-use regression model by [31] that used the same sample set and demonstrated a positive relationship between metal concentrations and the increasing population density, and a negative one with the amount of nearby forested areas. Some of the moss samples depart from the typical isotope ranges of urban emission sources and point towards higher $^{206}Pb/^{207}Pb$ ratios that are consistent with the Pb isotope signature of the resuspension of local and regional soils (terrigenous endmember; Fig. 3B). The study of the regional Corine Land Cover shows that 13 of our sampling sites, characterized by high Pb contents, are within 500 m of areas covered by > 50% of agricultural soils, which again supports the potential influence of Pb-contaminated resuspended soils in these areas. This conclusion is also perfectly in line with the findings of [70] on rural moss biomonitoring in France. [64] highlighted that Pb isotope ratios in aerosols in Paris had shifted from a dominant road traffic signature to an industrial one between 1995 and 2002 (Fig. 3A). Our results show that this trend was also recorded by our bioindicators and seems to persist two decades after. However, a slight discrepancy can be observed between the isotope signal in the 2002 aerosols and in this study. This isotope shift is particularly noticeable for samples with $^{208}Pb/^{206}Pb$ ratios < 2.103, i.e., sampling sites more susceptible to be impacted by a terrigenous source (agricultural and pre-industrial soils). The range of Pb isotope ratios varies as a function of distance from the city (Fig. 3B): samples collected within a 20 km-radius of Paris center present narrower $^{208}Pb/^{206}Pb$ and $^{206}Pb/^{207}Pb$ ratios than those collected farther than 20 km. This supports the hypothesis that a dominant source (or a constant mixing of sources) controls the atmospheric Pb in Paris and its closest outskirt, whereas additional emission sources contribute and can be isotopically detected at distances > 20 km.

### 3.5 Sources of atmospheric Pb and their relative contributions

Figure 4A reports the $^{206}Pb/^{207}Pb$ ratios measured in mosses against the reciprocal of their Pb enrichment factor ($EF_{Pb}$). In such diagram, binary mixing relationships are represented by straight lines [71]. Results show that Pb in all moss samples can be explained by a ternary mixing between three endmembers that have the following characteristics:

- The first endmember (EM1) is characterized by a low $^{206}Pb/^{207}Pb$ ratio (≤ 1.145) and a high $EF_{Pb} \geq 214$. Low $^{206}Pb/^{207}Pb$ are typical of the major Pb urban sources [23]. Samples collected within a 20 km radius from the city center are mostly impacted by this endmember. Unexpectedly, the sample most influenced by EM1 (sampling site 41) is located ~ 50 km south of Paris.
- the second endmember (EM2) has both high $^{206}Pb/^{207}Pb$ (≥ 1.170) and $EF_{Pb} \geq 214$. This high $^{206}Pb/^{207}Pb$ is coherent with the previously defined characteristics for agricultural and pre-industrial local and regional soil resuspension in France as well as emissions from cement factories [e.g., 73]. The sole cement factory in the study area is located 40 km northwest of Paris (the closest sampling site, site 57, is located 20 km from this factory). The cement used to make the tombstones or top walls on which mosses were collected may also be viewed as a potential source of Pb. This Pb would be expected to have a high $^{206}Pb/^{207}Pb$ (≥ 1.170; [72]). But the absence of correlation between Pb and Sr (Figure S1), an element naturally present in commercial cements [73], makes the tombstone a highly unlikely source of Pb in the mosses. Sampling sites that are the most impacted by this endmember were all collected more than 20 km away from Paris.
- the third endmember (EM3) is defined by some sampling sites that have $^{206}Pb/^{207}Pb$ ratios ranging between 1.156 and 1.164 (in particular, sampling sites 48 and 49) and moderate $EF_{Pb}$ (< 7). [74] reported a similar pattern for bioindicators in a Pyrenean Beech Forest between France and Spain and defined a background $^{206}Pb/^{207}Pb$ ratio of ~ 1.158 that matches the actual European atmospheric background, which also corresponds to our third mixing endmember. This third endmember represents a more remote source of atmospheric Pb compared to the other two.

#### 3.5.1 Estimating the relative contributions of the urban, terrigenous, and European background endmembers

To estimate the respective contributions from each of the three endmembers (EM1, EM2 and EM3) we used the MixSIAR Bayesian mixing model package in R. Results (Fig. 5) show that the EM1 (urban) and EM2 (terrigenous) endmembers are dominating atmospheric Pb in the Paris region with cumulative contributions close to 100% (Fig. 5A) for most sampling sites. Sampling sites within 20 km of the city center are mostly (≥ 50%) impacted by EM1, whereas

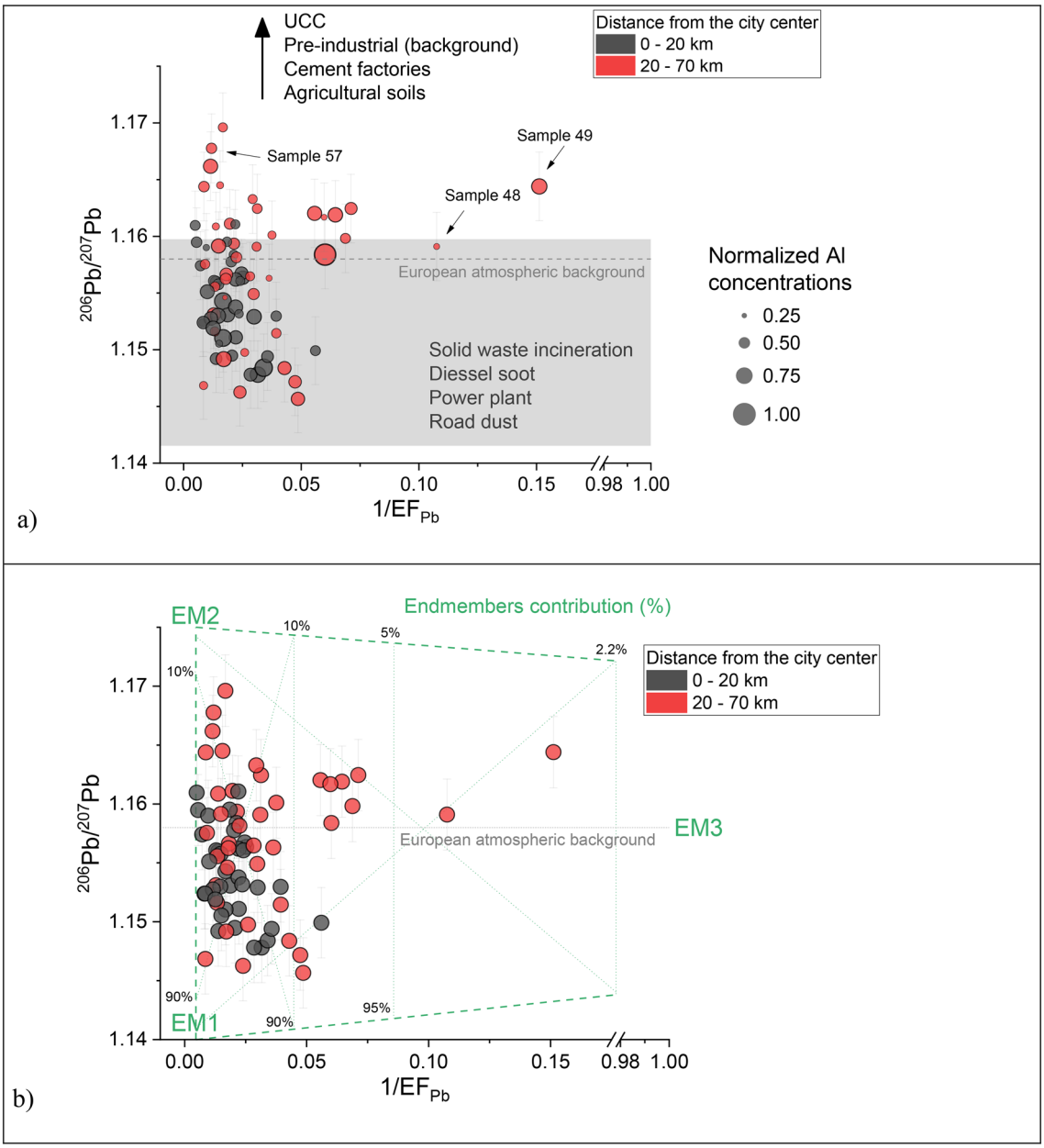



**Fig. 4.** $^{206}Pb/^{207}Pb$ vs. $1/EF_{Pb}$. **A** Moss samples. Aluminum concentrations in the moss samples are normalized to its highest measured concentration (i.e., $0 < Al$ normalized concentration $\leq 1$). **B** Ternary Isotope Balance Model (IBM). The characteristics considered for the three endmembers EM1 (Urban), EM2 (Terrigenous) and EM3 (European background) are detailed in the text

those farther than 20 km are evenly distributed between the EM1 and EM2 endmembers (Figs. 5B, C, D). As a whole, urban Pb accounts for 58 to 82% of the total Pb measured in the study area, as well as along a south-eastern corridor along the A6 motorway (Fig. 5B). Terrigenous Pb is more heterogeneously distributed in the study area. EM2 high contributions (48 to 58%) seems to originate from the north, north-west, south-west and north-east directions of Paris, which mostly correspond to agricultural areas (Fig. 5C).

Similar to what was observed in Fig. 4B, Fig. 5D indicates that the remote European background (EM3) does not significantly contribute to the atmospheric Pb concentrations in the study area (< ~ 5%). The two sampling sites (48 and 49) showing the highest contributions from EM3 are located about 40 and 60 km southwest of Paris, respectively (Fig. 5A). These sampling sites correspond to rural municipalities where over 95% of the land area is covered by agricultural, forestry and natural areas (Corine Land Cover).

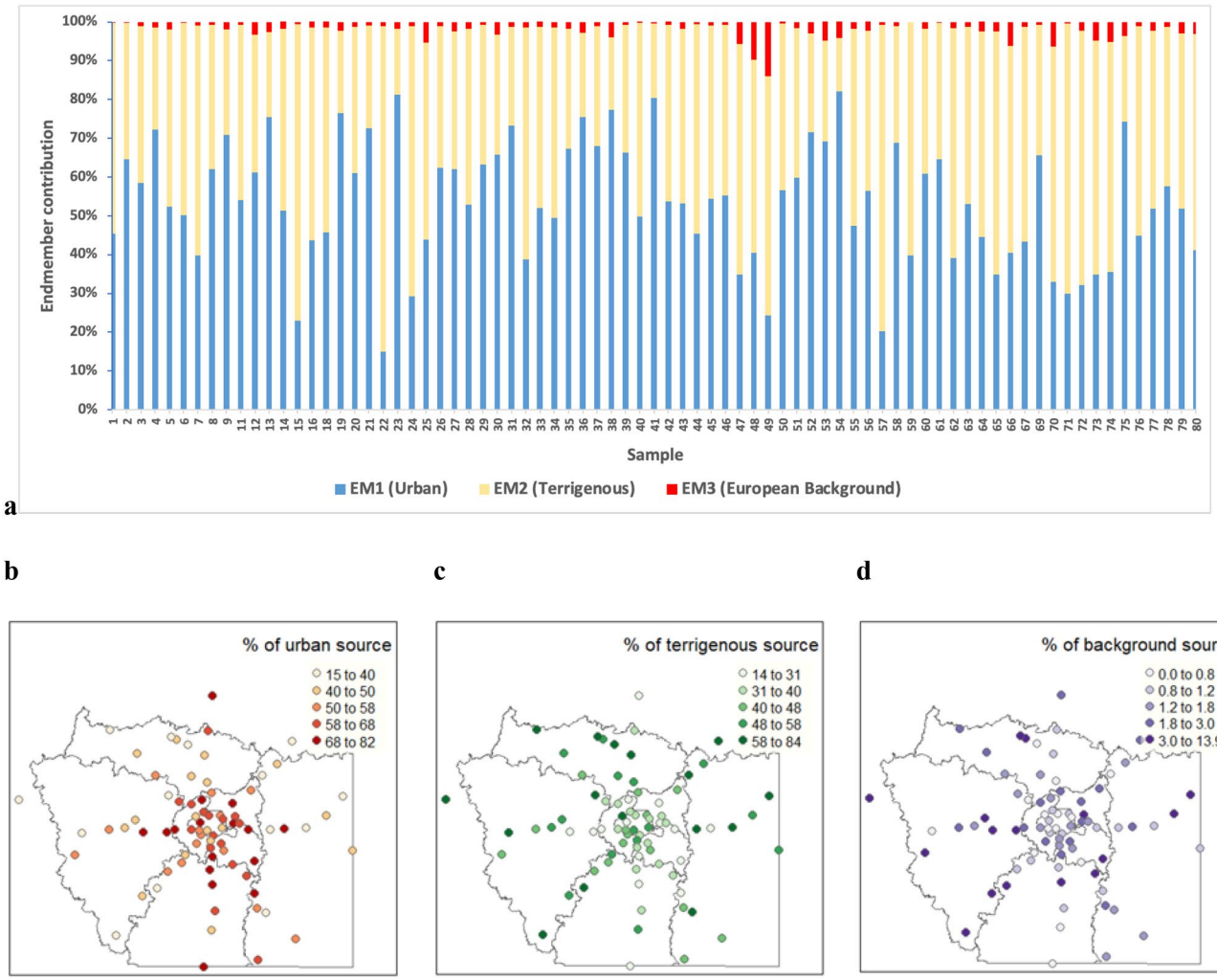



**Fig. 5** Estimation of the 3 endmembers respective contributions using the MixSIAR model (**A**). Spatial distributions of the endmembers contributions: EM1, urban (**B**), EM2, terrigenous (**C**) and EM3, European background (**D**)

### 3.5.2 Relationships between sources, metal concentrations and PCA component scores

Results from Table 3 reveal only modest Spearman correlations (0.44–0.47) between metals (Cu, Sb) and PC1 with the urban endmember EM1, and similar but negative correlation coefficients with the terrigenous endmember EM2. Only for the background endmember EM3, which only contributes < 15% to the atmospheric Pb budget in our study region, did we find a strong negative Spearman correlation coefficient (~ – 0.9) with Pb concentrations and Pb-related PC3. This indicates that Pb in our study did not come from the background sources.

## 4 Conclusions

Atmospheric particulate matter (PM) acts as a carrier for a wide range of contaminants. Here, using the example of the urban Parisian region, this study tested the potential for *Grimmia pulvinata* mosses collected in cemeteries (i.e., away from direct sources of contamination and only impacted by atmospheric deposition) to identify sources of atmospheric Pb and to quantify their respective contributions, by combining metal enrichment factors, principal component analysis and Pb isotope geochemistry. Altogether, these methods indicate that atmospheric Pb in the study region originates from three distinct types of sources: (i) the European atmospheric background that had been previously defined by [74], (ii) atmospheric particles emitted by regional urban sources and (iii) particles generated by the resuspension of

**Table 3** Correlation factors between endmembers (EM) contributions estimated by MixSIAR, metal concentrations and PCA component scores

| | %EM1 Urban | %EM2 Terrigenous | %EM3 European background |
|---|---|---|---|
| Al | 0.26 | − 0.25 | 0.07 |
| As | 0.19 | − 0.17 | − 0.11 |
| Cd | 0.35 | − 0.31 | **− 0.49** |
| Cr | 0.35 | − 0.32 | − 0.26 |
| Fe | 0.39 | − 0.37 | − 0.16 |
| Ni | 0.35 | − 0.33 | − 0.30 |
| Pb | 0.12 | − 0.05 | **− 0.91** |
| Sr | − 0.06 | 0.05 | 0.13 |
| V | 0.27 | − 0.26 | − 0.01 |
| Zn | 0.22 | − 0.18 | − 0.48 |
| Cu | **0.47** | **− 0.44** | − 0.33 |
| Sb | **0.47** | **− 0.44** | − 0.33 |
| PC1 | **0.44** | **− 0.42** | − 0.17 |
| PC2 | 0.16 | − 0.16 | 0.14 |
| PC3 | − 0.08 | 0.15 | **− 0.86** |
| PC4 | − 0.12 | 0.11 | 0.09 |

Bold values indicate significant correlation factors

regional soils. While *Grimmia pulvinata* samples were collected on tombstones or walls, our results show that cement, a constitutive element of concrete, is a highly unlikely source of Pb in cemetery mosses, thus not preventing using them as atmospheric metal bioindicators. Using isotope modelling, we estimated the respective contributions of these three endmembers for each sampling site. Among them, our results show that the European atmospheric background contributes the least, with most contributions < 5%, and that local urban and terrigenous sources are dominating. While urban sources display a spatial gradient from inner Paris towards its close and farther outskirts, the terrigenous sources do not exhibit a clear spatial pattern and as such remain more difficult to identify. *Grimmia pulvinata* is the most common species in the genus *Grimmia* and primarily lives in temperate regions, from sea level to altitudes of ~ 3000 m. This species will thus be ubiquitous in most of the urban environments facing air contamination by heavy metals. This makes it an excellent candidate to implement our approach to numerous cities and megacities around the world. This would ultimately allow to establish a standard method for biomonitoring metal air contamination in these environments, avoiding the eventual bias created by interchangeability issues between different bioindicator species.

**Acknowledgements** We are grateful to Nora Rouillier who sorted and prepared the moss samples.

**Author contributions** D.W.: Conceptualization, Methodology, Validation, Formal analysis, Investigation, Writing-original draft, Visualization, Supervision. C.M.: Conceptualization, Methodology, Validation, Formal analysis, Investigation, Writing-review and editing, Visualization. S.L.: Conceptualization, Methodology, Validation, Formal analysis, Investigation, Writing-review and editing, Visualization. E.P.S.: Formal analysis, Writing-review and editing, Visualization. E.L.: Conceptualization, Methodology, Validation, Formal analysis, Investigation, Writing-review and editing, Visualization, Funding acquisition. Y.M.G.: Formal analysis, Investigation, Writing-review and editing, Visualization.

**Funding** Moss collection and metal concentration analysis were funded by ANR (ANR-17-CE36-0005) in the framework of the Constances cohort (grant ANR-11-INBS-0002 from the French National Research Agency).

**Data availability** Data is provided within the manuscript or supplementary information files.

**Code availability** Not applicable.

## Declarations

**Competing interests** The authors declare no competing interests.

**Open Access** This article is licensed under a Creative Commons Attribution 4.0 International License, which permits use, sharing, adaptation, distribution and reproduction in any medium or format, as long as you give appropriate credit to the original author(s) and the source, provide a link to the Creative Commons licence, and indicate if changes were made. The images or other third party material in this article are included in the article's Creative Commons licence, unless indicated otherwise in a credit line to the material. If material is not included in the article's Creative Commons licence and your intended use is not permitted by statutory regulation or exceeds the permitted use, you will need to obtain permission directly from the copyright holder. To view a copy of this licence, visit http://creativecommons.org/licenses/by/4.0/.

## References

1. Cohen AJ, Brauer M, Burnett R, Anderson HR, Frostad J, Estep K, Balakrishnan K, Brunekreef B, Dandona L, Dandona R, Feigin V, Freedman G, Hubbell B, Jobling A, Kan H, Knibbs L, Liu L, Martin R, Morawska L, Pope CA, Shin H, Straif K, Shaddick G, Thomas M, van Dingenen R, van Donkelaar A, Vos T, Murray CJL, Forouzanfar MH. Estimates and 25-year trends of the global burden of disease attributable to ambient air pollution: an analysis of data from the Global Burden of Diseases Study 2015. The Lancet. 2017;389(100082):1907–18.
2. Filippelli G, Anenberg S, Taylor M, van Geen A, Khreis H. New approaches to identifying and reducing the global burden of disease from pollution. GeoHealth. 2020;4(4): e2018GH000167.
3. Mielke HW, Laidlaw MA, Gonzales CR. Estimation of leaded (Pb) gasoline's continuing material and health impacts on 90 US urbanized areas. Environ Int. 2011;37(1):248–57.
4. Yoshinaga J, Takagi M, Yamasaki K, Tamiya S, Watanabe C, Kaji M. Blood lead levels of contemporary Japanese children. Environ Health Prevent Med. 2012;17:27–33.
5. Grandjean P, Landrigan PJ. Neurobehavioural effects of developmental toxicity. Lancet Neurol. 2014;13(3):330–8.
6. Larsen B, Sánchez-Triana E. Global health burden and cost of lead exposure in children and adults: a health impact and economic modelling analysis. Lancet Planetary Health. 2023;7(10):e831–40.
7. Lovei M. Phasing out lead from gasoline: worldwide experience and policy implications (Vol. 397). World Bank Publications 1998.
8. Percival RV. Getting the lead out: the phase-out of gasoline lead additives—a global environmental success story. In The impact of environmental law. Edward Elgar Publishing;2020. pp. 8–29.
9. Shi T, Ma J, Zhang Y, Liu C, Hu Y, Gong Y, Wu X, Ju T, Hou H, Zhao L. Status of lead accumulation in agricultural soils across China (1979–2016). Environ Int. 2019;129:35–41.
10. Zahran S, Laidlaw MA, McElmurry SP, Filippelli GM, Taylor M. Linking source and effect: resuspended soil lead, air lead, and children's blood lead levels in Detroit, Michigan. Environ Sci Technol. 2013;47(6):2839–45.
11. Lequy E, Leblond S, Siemiatycki J, Meyer C, Vienneau D, de Hoogh K, Zins M, Goldberg M, Jacquemin J. Long-term exposure to airborne metals and risk of cancer in the French cohort Gazel. Environ Int. 2023;177: 107999.
12. Rühling Å, Skärby L. Landsomfattande kartering av regionala tungmetallhalter i mossa. National survey of regional heavy metal concentrations in moss. Statens naturvårdsverk. 1979;PM 1191:1–28.
13. Bargagli R. Moss and lichen biomonitoring: a review. Sci Total Environ. 2016;572:216–31.
14. Wu Q, Wang X, Zhou Q. Biomonitoring persistent organic pollutants in the atmosphere with mosses: performance and application. Environ Int. 2014;66:28–37.
15. Jiang Y, Fan M, Hu R, Zhao J, Wu Y. Mosses are better than leaves of vascular plants in monitoring atmospheric heavy metal pollution in urban areas. Int J Environ Res Public Health. 2018;15:1105.
16. Dietrich M, Krekeler MP, Kousehlar M, Widom E. Quantification of Pb pollution sources in complex urban environments through a multi-source isotope mixing model based on Pb isotopes in lichens and road sediment. Environ Pollut. 2021;288: 117815.
17. Shi C, He H, Xia Z, Gan H, Xue Q, Cui Z, Chen J. Heavy metals and Pb isotopes in a marine sediment core record environmental changes and anthropogenic activities in the Pearl River Delta over a century. Sci Total Environ. 2022;814: 151934.
18. Jeong H, Ra K. Multi-isotope signatures (Cu, Zn, Pb) of different particle sizes in road-deposited sediments: a case study from industrial area. J Anal Sci Technol. 2021;12:1–14.
19. Widory D, Vautour G, Poirier A. Atmospheric dispersion of trace metals between two smelters: an approach coupling lead, strontium and osmium isotopes from bioindicators. Ecol Ind. 2018;84:497–506.
20. Sensuła B, Fagel N, Michczyński A. Radiocarbon, trace elements and Pb isotope composition of pine needles from a highly industrialized region in southern Poland. Radiocarbon. 2021;63:713–26.
21. Ciężka M, Górka M, Stojanowska A, Modelska M, Łubek A, Widory D. Air quality in the Świętokrzyski National Park (Poland) viewed through the multi-isotope geochemistry (S, C, N and Pb) of *Hypogymnia physodes* lichens: sources, seasonality and dynamics. Isot Environ Health Stud. 2022. https://doi.org/10.1080/10256016.2022.2110591.
22. Bagur M, Widory D. Characterizing the levels and sources of the historical metal contamination in the atmosphere of Montreal (Canada) from 1973 to 2013 by coupling chemistry and lead and osmium isotope ratios. Atmos Res. 2020. https://doi.org/10.1016/j.atmosres.2019.104794.
23. Jung CC, Chou CCK, Huang YT, Chang SY, Lee CT, Lin CY, Cheung HC, Kuo WC, Chang CW, Chang SH. Isotopic signatures and source apportionment of Pb in ambient $PM_{2.5}$. Sci Rep. 2022;12:4343.
24. Cheema AI, Liu G, Yousaf B, Abbas Q, Zhou H. A comprehensive review of biogeochemical distribution and fractionation of lead isotopes for source tracing in distinct interactive environmental compartments. Sci Total Environ. 2020;719: 135658.
25. Schnyder E, Strok M, Kosonen Z, Skudnik M, Mazej D, Jeran Z, Thöni L. Lead concentrations and stable lead isotope ratios in moss in Slovenia and Switzerland. Ecol Ind. 2018;95:250–9. https://doi.org/10.1016/j.ecolind.2018.06.072.
26. Sucharova J, Suchara I, Hola M, Reimann C. Contemporary lead concentration and stable lead isotope ratio distribution in forest moss across the Czech Republic. Appl Geochem. 2014;40:51–60. https://doi.org/10.1016/j.apgeochem.2013.10.012.
27. Haack U, Kienholz B, Reimann C, Schneider J, Stumpfl EF. Isotopic composition of lead in moss and soil of the European Arctic. Geochim Cosmochim Acta. 2004;68(12):2613–22. https://doi.org/10.1016/j.gca.2003.12.019.

28. Zhou X, Hu R, Fang Y. Source and spatial distribution of airborne heavy metal deposition studied using mosses as biomonitors in Yancheng, China. Environ Sci Pollut Res. 2021;28:30758–73. https://doi.org/10.1007/s11356-021-12814-z.
29. Deljanin I, Antanasijević D, Vuković G, Urošević MA, Tomašević M, Perić-Grujić A, Ristić M. Lead spatio-temporal pattern identification in urban microenvironments using moss bags and the Kohonen self-organizing maps. Atmos Environ. 2015;117:180–6.
30. Oishi Y. Moss biomonitoring using lead isotope ratios requires careful attention: evaluation of transboundary pollutants in Japan. Atmos Environ. 2022;275: 119004.
31. Lequy E, Meyer C, Vienneau D, Berr C, Goldberg M, Zins M, Leblond S, de Hoogh K, Jacquemin B. Modeling exposure to airborne metals using moss biomonitoring in cemeteries in two urban areas around Paris and Lyon in France. Environ Pollut. 2022. https://doi.org/10.1016/j.envpol.2022.119097.
32. Vieille B, Albert I, Leblond S, Couvidat F, Parent E, Meyer C. Are Grimmia mosses good biomonitors for urban atmospheric metallic pollution? Preliminary evidence from a French case study on cadmium. Atmosphere. 2021;12:491. https://doi.org/10.3390/atmos12040491.
33. Natali M, Zanella A, Rankovic A, Banas D, Cantaluppi C, Abbadie L, Lata JC. Assessment of trace metal air pollution in Paris using slurry-TXRF analysis on cemetery mosses. Environ Sci Pollut Res. 2016;23:23496–510. https://doi.org/10.1007/s11356-016-7445-z.
34. Ugur A, Özden B, Saç MM, Yener G. Biomonitoring of $^{210}$Po and $^{210}$Pb using lichens and mosses around a uriniferous coal-fired power plant in western Turkey. Atmos Environ. 2003;37:2237–45.
35. Gallego-Cartagena E, Morillas H, Carrero JA, Madariaga JM, Maguregui M. Naturally growing grimmiaceae family mosses as passive biomonitors of heavy metals pollution in urban-industrial atmospheres from the Bilbao Metropolitan area. Chemosphere. 2021;263: 128190. https://doi.org/10.1016/j.chemosphere.2020.128190.
36. Brigaud B, Vincent B, Pagel M, Gras A, Noret A, Landrein P, Huret E. Sedimentary architecture, depositional facies and diagenetic response to intracratonic deformation and climate change inferred from outcrops for a pivotal period (Jurassic/Cretaceous boundary, Paris Basin, France). Sediment Geol. 2018;373:48–76.
37. Steinnes E, Ruhling A, Lippo H, Makinen A. Reference materials for large-scale metal deposition survey. Accred Qual Assur. 1997;2:243–9. https://doi.org/10.1007/s007690050141.
38. Belshaw NS, Freedman PA, O'nions RK, Frank M, Guo Y. A new variable dispersion double-focusing plasma mass spectrometer with performance illustrated for Pb isotopes. Int J Mass Spectrom. 1998;181:51–8.
39. Woodhead JD, Hergt JM. Pb-isotope analyses of USGS reference materials. Geostand Newsl. 2000;24(1):33–8.
40. Weis D, Kieffer B, Maerschalk C, Pretorius W, Barling J. High-precision Pb-Sr-Nd-Hf isotopic characterization of USGS BHVO-1 and BHVO-2 reference materials. Geochem Geophys Geosyst. 2005. https://doi.org/10.1029/2004GC000852.
41. Aebischer S, Cloquet C, Carignan J, Maurice C, Pienitz R. Disruption of the geo-chemical metal cycle during mining: multiple isotope studies of lake sediments from Schefferville, subarctic Québec. Chem Geol. 2015;412:167–78.
42. Sinex SA, Helz GR. Regional geochemistry of trace elements in Chesapeake Bay sediments. Environ Geol. 1981;3:315–23. https://doi.org/10.1007/BF02473521.
43. Zoller W, Gladney ES, Duce RA. Atmospheric concentrations and sources of trace metals at the South Pole. Science. 1974;183:198–200.
44. Chatterjee M, Silva FE, Sarkar SK. Distribution and possible source of trace elements in the sediment cores of a tropical macrotidal estuary and their ecotoxicological significance. Environ Int. 2007;33:346–56.
45. Wedepohl KH. The composition of the continental crust. Geochim Cosmochim Acta. 1995;59(7):1217–32.
46. Chen CW, Kao CM, Chen CF, Dong CD. Distribution and accumulation of heavy metals in the sediments of Kaohsiung Harbor, Taiwan. Chemosphere. 2007;66:1431–40.
47. Betha R, Behera SN, Balasubramanian R. 2013 Southeast Asian smoke haze: fractionation of particulate-bound elements and associated health risk. Environ Sci Technol. 2014;48:4327–35.
48. Lyu Y, Zhang K, Chai F. Atmospheric size-resolved trace elements in a city affected by non-ferrous metal smelting: indications of respiratory deposition and health risk. Environ Pollut. 2017;224:559–71.
49. Douglas J, Schilling JG. Systematics of three-component, pseudo-binary mixing lines in 2D isotope ratio space representations and implications for mantle plume-ridge interaction. Chem Geol. 2000;163:1–23.
50. Stock BC, Jackson AL, Ward EJ, Parnell AC, Phillips DL, Semmens BX. Analyzing mixing systems using a new generation of Bayesian tracer mixing models. PeerJ. 2018;6: e5096.
51. Phillips DL, Inger R, Bearhop S, Jackson AL, Moore JW, Parnell AC, Semmens BX, War EJ. Best practices for use of stable isotope mixing models in food-web studies. Can J Zool. 2014;92:823–35.
52. Lin CC, Chen SJ, Huang KL, Hwang WI, Chang-Chien GP, Lin WY. Characteristics of metals in nano/ultrafine/fine/coarse particles collected beside a heavily trafficked road. Environ Sci Technol. 2005;39:8113–22.
53. PlasenciaSánchez E, Sánchez-Soberón F, Rovira J, Sierra J, Schuhmacher M, Soler A, Torrentó C, Rosell M. Integrating dual C and N isotopic approach to elemental and mathematical solutions for improving the PM source apportionment in complex urban and industrial cities: Case of Tarragona—Spain. Atmospheric Environ. 2023;293: 119449.
54. Frontasyeva M, Harmens H, Uzhinskiy A, Chaligava O. Mosses as biomonitors of air pollution: 2015/2016 survey on heavy metals, nitrogen and POPs in Europe and Beyond. Report of the ICP Vegetation Moss Survey Coordination Centre, Joint Institute for Nuclear Research, Dubna, Russian Federation 2020; 136 pp. ISBN 978-5-9530-0508-1.
55. Jomova K, Jenisova Z, Feszterova M, Baros S, Liska J, Hudecova D, Rhodes CJ, Valko M. Arsenic: toxicity, oxidative stress and human disease. J Appl Toxicol. 2011;31(2):95–107.
56. Påhlsson AMB. Toxicity of heavy metals (Zn, Cu, Cd, Pb) to vascular plants. Water Air Soil Pollut. 1989;47:287–319.
57. Straif K, Benbrahim-Tallaa L, Baan R, Grosse Y, Secretan B, El Ghissassi F, Bouvard V, Guha N, Freeman C, Galichet L, Cogliano V. A review of human carcinogens-Part C: metals, arsenic, dusts, and fibres. Lancet Oncol. 2009;10(5):453–4.
58. Vlastelic I, Suchorski K, Sellegri K, Colomb A, Nauret F, Bouvier L, Piro JL. The trace metal signature of atmospheric aerosols sampled at a European regional background site (puy de Dôme, France). J Atmos Chem. 2014;71:195–212.
59. Agnan Y, Séjalom-Delmas N, Claustres A, Probst A. Investigation of spatial and temporal metal atmospheric deposition in France through lichen and moss bioaccumulation over one century. Sci Total Environ. 2015;529:285–96.

60. Doucet FJ, Carignan J. Atmospheric Pb isotopic composition and trace metal concentration as revealed by epiphytic lichens: an investigation related to two altitudinal sections in Eastern France. Atmos Environ. 2001;35:3681–90.
61. Monna F, Bouchaou I, Rambeau C, Losno R, Bruguier O, Dongarrà G, Black S, Chateau C. Lichens used as monitors of atmospheric pollution around Agadir (Southwestern Morocco)—a case study predating lead-free gasoline. Water Air Soil Pollut. 2012;223:1263–74.
62. Le Galley E, Widom E, Krekeler MPS, Kuentz DC. Chemical and lead isotope constraints on sources of metal pollution in street sediment and lichens in southwest Ohio. Appl Geochem. 2013;32:195–203.
63. Souto-Oliveira CE, Babinski M, Araújo DF, Weiss DJ, Ruiz IR. Multi-isotope approach of Pb, Cu and Zn in urban aerosols and anthropogenic sources improves tracing of atmospheric pollutant sources in megacities. Atmos Environ. 2019;198:427–37.
64. Widory D, Roy S, Le Moullec Y, Goupil G, Cocherie A, Guerrot C. The origin of atmospheric particles in Paris: a view through carbon and lead isotopes. Atmos Environ. 2004;38:953–61.
65. Froger C, Ayrault S, Evrard O, Monvoisin G, Bordier L, Lefèvre I, Quantin C. Tracing the sources of suspended sediment and particle-bound trace elements in an urban catchment coupling elemental and isotopic geochemistry, and fallout radionuclides. Environ Sci Pollut Res. 2018;25:28667–81.
66. Glorennec P, Azema A, Durand S, Ayrault S, Le Bot B. The isotopic signature of lead emanations during the fire at Notre Dame Cathedral in Paris, France. Environ Res Public Health. 2021;18:5420.
67. Millot R, Allègre CJ, Gaillardet J, Roy S. Lead isotopic systematics of major river sediments: a new estimate of the Pb isotopic composition of the Upper Continental Crust. Chem Geol. 2004;203:75–90.
68. Carignan J, Libourel G, Cloquet C, Le Forestier L. Lead isotopic composition of fly ash and flue gas residues from municipal solid waste combustors in France: implications for atmospheric lead source tracing. Environ Sci Technol. 2005;39:2018–24.
69. Lahd Geagea M, Stille P, Gauthier-Lafaye F, Millet M. Tracing of industrial aerosol sources in an urban environment using Pb, Sr, and Nd isotopes. Environ Sci Technol. 2008;42(3):692–8.
70. Lequy E, Saby N, Ilyin I, Bourin A, Sauvage S, Leblond S. Spatial analysis of trace elements in a moss bio-monitoring data over France by accounting for source, protocol and environmental parameters. Sci Total Environ. 2017;590–591:602–10.
71. Langmuir CH, Vocke RD, Hanson GN. A general mixing equation with application to Icelandic basalts. Earth Planet Sci Lett. 1978;37:380–92.
72. Semlali RM, Van Oort F, Denaix L, Loubet M. Estimating distributions of endogenous and exogenous Pb in soils by using Pb isotopic ratios. Environ Sci Technol. 2001;35:4180–8.
73. Kittnerová J, Drtinová N, Štamberg K, Vopálka D, Evans N, Deissmann G, Lange S. Comparative study of radium and strontium behaviour in contact with cementitious materials. Appl Geochem. 2020;122: 104713.
74. Barre JPG, Queipo-Abad S, Sola-Larrañaga C, Deletraz G, Bérail S, Tessier E, Elustondo Valencia D, Santamaría JM, de Diego A, Amouroux D. Comparison of the isotopic composition of Hg and Pb in two atmospheric bioaccumulators in a Pyrenean Beech Forest (Iraty Forest, Western Pyrenees, France/Spain). Front Environ Chem. 2020. https://doi.org/10.3389/fenvc.2020.582001.

**Publisher's Note** Springer Nature remains neutral with regard to jurisdictional claims in published maps and institutional affiliations.